Available online at www.sciencedirect.com
ScienceDirect
International Journal of Pharmaceutics 321 (2006) 108–116
INTERNATIONAL JOURNAL OF PHARMACEUTICS
www.elsevier.com/locate/ijpharm

# Formation of hollow core granules by fluid bed in situ melt granulation: Modelling and experiments

Mansoor A. Ansari, Frantisek Stepanek *

*Department of Chemical Engineering, Imperial College London, South Kensington Campus, London SW7 2AZ, United Kingdom*

Received 10 February 2006; received in revised form 2 May 2006; accepted 5 May 2006
Available online 16 May 2006

**Abstract**

Granules with a characteristic core–shell internal structure have been formed by in situ melt fluid-bed granulation, using D-mannitol primary solid particles and poly-ethylene glycol (PEG-6000) binder. The effect of binder particle size and binder/solids ratio on granule size distribution was systematically investigated. The mean granule size was found to be directly proportional to the binder particle size. The binder amount did not measurably affect the granule size, only the fraction of un-granulated fines. The microstructure of the granules was analysed by X-ray micro-tomography; the average shell thickness in the granules was found to depend on the binder/solids ratio, and the core volume was found to be directly proportional to the binder particle size. However, for binder particle size below a certain value the core–shell structure disappeared. A mathematical model based on a layering growth mechanism has been proposed and found to be consistent with experimental data. The proposed growth mechanism was confirmed by creating granules with bi-modal size distribution using a mixture of differently sized binder seeds.


*Keywords:* Fluid-bed granulation; X-ray micro-tomography; Granule structure; Particle size; Melt binder; Nucleation; Regime separation

## 1. Introduction

The purpose of a granulation process is to form larger particles (granules) from a fine powder, while maintaining good control of the size and internal microstructure of the product. Granulation is typically achieved by mixing primary solid particles with a liquid binder. In fluid bed granulation, this mixing is achieved by the upward flow of a fluidising gas, which also provides a means of controlling the evaporation (for solution binders) and heating or cooling (for melt binders) rates (Turton et al., 1999). The binder is usually added to the fluid bed in the form of a fine spray by means of an atomising nozzle. In that case the average droplet size tends to be smaller than the primary particle size. An alternative method, suitable for melt binders, is to add the binder in solid form as flakes or discrete particles and create a liquid in situ after raising the process temperature above the melting point of the binder. In that case any ratio of droplet to particle size can in principle be achieved (subject to limits on fluidisation and particle entrainment). While in situ melt binders have been used in high-shear granulation processes for some time, their use in fluid-bed granulation is relatively recent (Abberger, 2001; Walker et al., 2005).

In broad terms any particle build-up process may be described as a combination of three sets of rate processes, namely wetting and nucleation, consolidation and growth, and attrition and breakage (Iveson et al., 2001). The final granule size distribution is the net result of the rates of these three processes, which has led to the idea of achieving good control over granule size distribution by regime-separated granulation (Litster, 2003), i.e., the physical de-coupling of the individual stages, particularly nucleation and growth. The use of in situ melt binders is, in effect, one possible way of realising this regime separation since the size of the binder particles that serve as nuclei can be determined externally to the granulation process and the onset of melting can be directly controlled by the process temperature.

For in situ melt binders in high shear mixers, two different nucleation mechanisms – called distribution and immersion – have been proposed depending on the relative size of binder to solid particles (Schæfer and Mathiesen, 1996). Distribution of the molten binder on the surface of primary solids may occur if the size of binder particles is comparable to or smaller than that of primary solid particles. The binder-covered primary

* Corresponding author. Tel.: +44 20 7594 5608; fax: +44 20 7594 5604.
*E-mail address:* f.stepanek@imperial.ac.uk (F. Stepanek).

0378-5173/$ – see front matter © 2006 Elsevier B.V. All rights reserved.
doi:10.1016/j.ijpharm.2006.05.012

**Nomenclature**

| | |
|---|---|
| $c$ | core compaction ratio, dimensionless |
| $d$ | diameter (m) |
| $m$ | mass (kg) |
| $V$ | volume ($m^3$) |
| $w_{fines}$ | volume fraction of fines, dimensionless |
| $x_{b/s}$ | volumetric binder/solids ratio in the shell, dimensionless |
| $x_{sat}$ | relative pore-space saturation, dimensionless |

*Subscripts and superscripts*

| | |
|---|---|
| b | binder |
| core | related to the core region of granule |
| g | granule |
| s | solids |
| shell | related to the shell region of granule |
| tot | total |

*Greek symbols*

| | |
|---|---|
| $\rho$ | density ($kg\,m^{-3}$) |
| $\psi$ | packing density of primary solid particles, dimensionless |

particles subsequently form granules by coalescence. On the other hand, if the binder particles are larger than the primary powder, immersion of primary particles into the molten binder particles and subsequent layering would dominate the granule growth process. In analogy, the effect of liquid binder droplet size on growth mechanisms in fluid-bed melt granulation has been studied (Schæfer and Wørts, 1978; Abberger et al., 2002) and growth mechanisms consistent with those in high shear mixers have been observed (cf. also a recent review article by Mort (2005) and references therein).

The objective of the present work was to perform a systematic study of the effect of the binder to particle size ratio and the binder to solids mass ratio on the size distribution and internal microstructure of granules formed by in situ melt granulation in a fluid bed process, and to formulate and validate a model allowing quantitative explanation of the relationship between binder particle size, binder to solids ratio, and the final granule attributes. The paper is structured as follows. First, the materials used for granule preparation and methods employed in granule characterisation are described. The experimental results of the effect of binder to solids ratio and the binder to particle size ratio on the size distribution and internal microstructure of the granular product are presented and discussed next. A mathematical model is then formulated and its predictions compared with the experimentally observed trends.

## 2. Materials and methods

### 2.1. Granule preparation

Granules for this study were prepared by fluid bed granulation from D-mannitol "Pearlitol-200SD" (Roquette, France) primary particles and poly-ethylene glycol (PEG- 6000, VWR, UK) binder. D-Mannitol is a common pharmaceutical excipient, used in particular in orally disintegrating tablet formulations (Bogner and Wilkosz, 2002; Kaushik et al., 2004). PEG is a typical example of a melt binder, allowing a range of melting points and melt viscosities depending on the mean molecular weight (for PEG-6000 the melting point is around 58–60 °C). Solid PEG was milled and sieved into size fractions; the 106–250, 250–355, 355–500, and 500–710 μm size fractions (further referred to as S, M, L, and XL, respectively) were used in granulation. The mannitol used for granulation was a spray-dried powder that was also sieved into a narrow size fraction as specified in Table 1. The relative size of binder and primary solid particles was deliberately chosen such that the binder particles are larger than those of the primary solids. This arrangement is central to the formation of hollow-core granules by the immersion and layering growth mechanism, which will be discussed in detail in Section 3.3 below. A relatively narrow size fraction of mannitol primary particles was used in order to avoid size segregation and fines entrainment during fluidisation. A secondary effect of using a narrow primary particle size range was that the primary particle packing in the granule approached the close random packing limit, as can be seen on a SEM micrograph of typical granules, shown in Fig. 1.

Table 1
Size distribution of mannitol primary solid particles

| Mannitol sieve cut (μm) | wt.% |
|---|---|
| Part > 350 | 0.0 |
| Part > 250 | 7.7 |
| Part 150–250 | 68.6 |
| Part < 150 | 23.7 |
| Part < 100 | 0.0 |

Granulation was performed in a desktop fluidised bed granulator of the "4M8" range (Pro-C-epT, Belgium) equipped with computer logging of process parameters. A single granulation experiment consisted of three steps: mixing, heating, and cooling. A 200 g batch composed of mannitol and PEG particles in

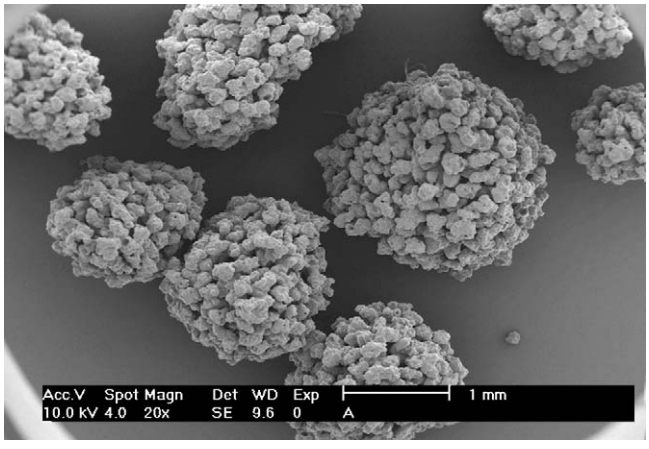


Fig. 1. SEM micrograph of several typical mannitol granules prepared by in situ melt fluid bed granulation with PEG binder.

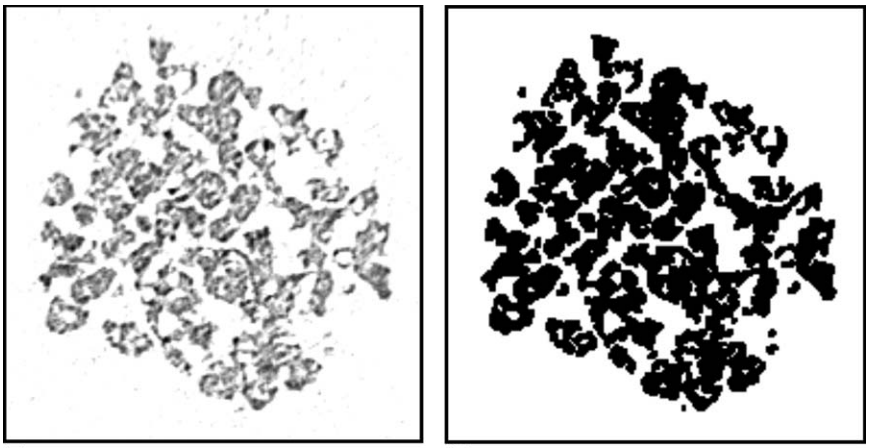


Fig. 2. Example of image enhancement using the ImageJ software. (a) Original X-ray image and (b) enhanced image.

the chosen ratio was first fluidised at ambient temperature for approximately 120 s to achieve mixing. The inlet air flow-rate was kept in the range of 0.5–0.6 $m^3$/min. Temperature of the bed was then raised at the rate of 7–10 °C/min to 60–65 °C (i.e., just above the melting point of the PEG binder) and maintained at the same level for 120 s. Agglomeration occurred at this stage. Finally, the bed was gradually cooled down to 40 °C before discharging.

### 2.2. Particle size and microstructure analysis

The particle size measurements were performed by automated image analysis of approximately 5000 particles of each well-mixed sample using Ankersmid DSA-10 size and shape analyser. Granule microstructure was characterised by means of X-ray computed micro-tomography (XMT) (Farber et al., 2003), using the SkyScan 1072 desktop X-ray micro-tomograph (SkyScan, Belgium). Granule samples were scanned using a 0.9° scan step from 0° to 180° and the typical acquisition time was around 45 min. Cross-sectional pixel size of 3.66 μm was maintained for all samples. Cross-sectional and three-dimensional images were reconstructed using the SkyScan software package. Each hollow-core granule image was segmented into its core and shell regions. The volume of core within the granule was approximated using a best-fit sphere as a region of interest (ROI).

Selected two-dimensional horizontal tomographic images of granules were further processed by the image processing software ImageJ. Due to the different noise level and the correction requirement, the tools used for enhancement were not identical with all images. However, the set of operations for image enhancement was confined to threshold adjustment, de-speckle, fill holes, dilate, erode and again fill holes if necessary. Both dilate and erode operations were used for equal number of times to maintain the phase volume and external dimensions of the cross-sections. An example illustrating a granule XMT image before and after enhancement is given in Fig. 2. Only enhanced images will further be shown.

## 3. Results and discussion

### 3.1. Effect of binder particle size on granule size and microstructure

First, let us investigate the effect of binder particle size on the size and microstructure of granules. Granules were prepared according to the protocol described in Section 2.1 from mannitol particle size fraction of 150–250 μm and all four binder particle size ranges using a constant binder to solids mass ratio of 0.18 g/g. The cumulative volume-weighted particle size distributions of the resulting granules are plotted in Fig. 3. As the figure reveals, there is clearly a direct correlation between the binder particle size and the resulting granule size. The mean equivalent granule diameter was 445, 566, 789, and 989 μm in the four cases. The fact that there is such a strong correlation between the binder particle size and the resulting granule size is indicative of the immersion mechanism mentioned in the Introduction, i.e., each binder particle is thought to have served as a nucleus for a single granule, and granule growth occurred by

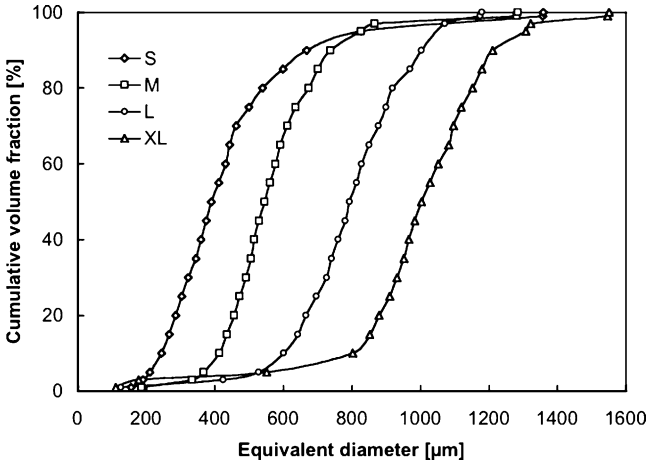


Fig. 3. Cumulative volume-weighted granule size distribution as function of binder particle size for constant total binder to solids mass ratio of 0.18.

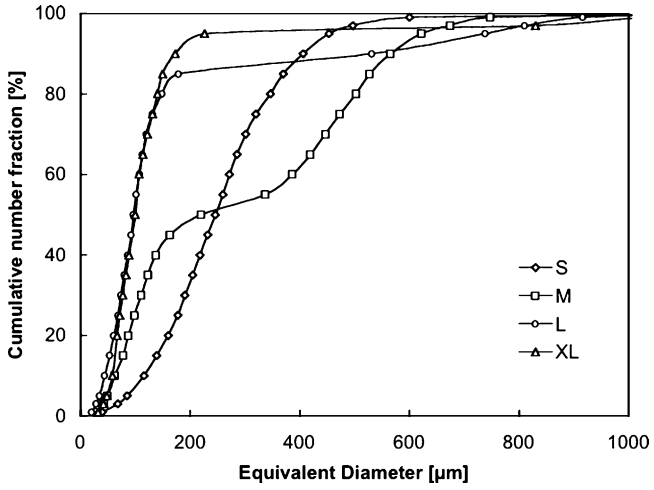


Fig. 4. Cumulative number-weighted granule size distribution as function of binder particle size for constant binder to solids mass ratio of 0.18.

a gradual build-up of layers of primary solid particles on the surface of the nucleus (Schæfer and Mathiesen, 1996).

A further indication of the layering growth mechanism is provided by the number-based granule size distribution, plotted in Fig. 4. The number distributions may be viewed as a mirror image of volume distributions (Fig. 3), because the order of the curves is nearly opposite. In Fig. 4 we can see that with increasing the mean binder particle size from 178 μm (S) to 605 μm (XL), the number fraction of un-granulated primary particles in the final product is increasing as well, although granules dominate the system by volume as is shown in Fig. 3. Under the layering mechanism, a larger binder particle size for a constant binder-to-solids ratio means that a smaller number of binder particles are available to serve as nuclei for a given number of primary solid particles. Consequently, the number fraction of any un-granulated fines remaining in the system should become larger. This trend is indeed revealed by Fig. 4—as the binder particle size increases from S to XL, a shift in the number-based size distribution towards smaller values occurs. The distributions are tending toward an asymptotic limit, namely the number distribution of the primary particles alone. Notice also the interesting (bi-modal) transition case realised by binder size M. The comparison of volume- and number-based distributions of the same samples indicates that a balance between the binder particle size, the required granule size and the number ratio of binder particles to primary solids would be imperative for process optimisation. The effect of the binder ratio on the fraction of un-granulated fines will be further discussed in Section 3.2 below.

Granule internal microstructure was analysed in order to obtain further insight into the assumed growth mechanism. The enhanced tomographic images showing the horizontal cross-sections at different position within each granule are presented in Fig. 5. Granules in the size range of 500–800 μm were chosen

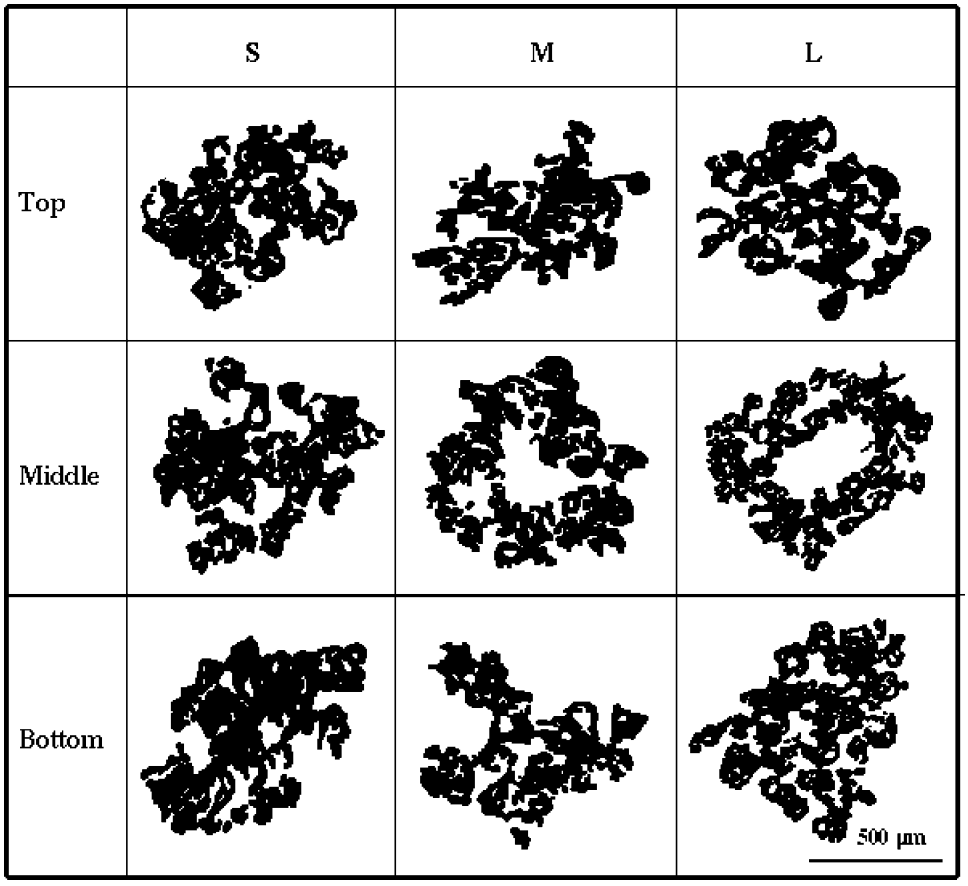


Fig. 5. Enhanced 2D horizontal X-ray images of mannitol granules prepared using three different PEG binder particle sizes as indicated in the column header. The top and bottom slices have been selected approximately 150 μm inside the granule from the top and bottom end.

Table 2
Comparison of binder particle size with resulting core and granule dimensions evaluated from tomography images

| Binder size code | Binder size range (μm) | Equivalent core diameter (μm) | Maximum core diameter (μm) | Maximum granule diameter (μm) |
|---|---|---|---|---|
| M | 250–355 | 199 | 361 | 999 |
| M | 250–355 | 217 | 303 | 832 |
| M | 250–355 | 226 | 338 | 823 |
| L | 355–500 | 326 | 513 | 1091 |
| L | 355–500 | 352 | 455 | 1073 |
| L | 355–500 | 403 | 488 | 1036 |

from each batch for the purpose of this tomographic analysis. Several interesting trends are noticeable: granule structure is quite open and porous which is usually the case in fluid-bed granulation. When the binder size was comparable with the primary solids (binder size S) there was no marked structural difference in the top, middle and bottom slices of the granule. But for the granules prepared with relatively coarser binder particles (columns labelled M and L), the images unfold the existence of a hollow core inside the granule. The volume of these cores appears to be an increasing function of the binder particle size.

The core volume of three randomly selected granules from batches prepared with M and L size binders were evaluated from their three-dimensional tomographic images using the best-fit sphere method. These measurements were not possible for the batch prepared with the S size binder as no distinctive core was observed in the corresponding randomly selected three granules. Due to slight asphericity of the cores, the criterion of choosing the best sphere was based on the solid fraction of $\leq$15% within the region of interest (ROI) covered by the sphere. The diameter of the covering sphere for each core was recorded. Their comparison with the binder particle size ranges is shown in Table 2. Due to the irregular core shape, the maximum core diameter (Ferret) is also reported in the table, as well as the maximum granule diameter measured from the X-ray images. The correspondence between the binder particle size, the core diameter, and the granule size, as well as the scale of individual variations within each group of three granules, is demonstrated by the values reported in the table. The key conclusions from the core volume analysis are that: (i) both core and granule diameters are correlated with the binder particle diameter; (ii) the equivalent core diameter is generally smaller than that of the original binder particle, due to the initial immersion of particles in to the molten binder surface, possibly followed by further compaction; (iii) based on the three samples in each case, the relative spread of core diameters for a given binder particle size appears to be larger than that of the final granule diameters. From the statistical point of view of course, one has to bear in mind that these conclusions are based on a very small sample. Unfortunately, the time-consuming nature of XMT analysis using present-day instruments does not permit otherwise.

The microstructure study was complemented by the tomographic analysis of granules prepared from the same, L size, binder but belonging to different size classes. The cross-sections of enhanced X-ray micrographs at the mid-point of each granule are shown in Fig. 6. The important finding is that the presence of the hollow core was observed in all chosen size classes. One can also notice the existence of multi-core structures apparent in some of the larger granules. This was perhaps the result of the agglomeration of growing nuclei that were originally following the immersion growth mechanism but instead of acquiring only primary particles on their surface, they coalesced after collision.

### 3.2. *Effect of binder ratio on granule size distribution*

So far we have seen that granule size can be controlled by the binder particle size for a fixed binder-to-solids ratio (Fig. 3), and that the binder particle size also has a strong effect on the number fraction of un-granulated fines (Fig. 4). Let us now investigate the influence of the other important parameter, namely the binder-to-solids ratio, on the granule size distribution and the fraction of fines. To this effect, granulation experiments with a fixed binder particle size L (i.e., size range of 355–500 μm) and four values of the binder-to-solids ratio equal to 0.05, 0.11, 0.18, and 0.25 g/g were performed. The cumulative volume-based size distributions of the resulting granules are plotted in Fig. 7. Several interesting trends are noticeable from the figure. First, there is a considerable fraction of un-granulated fines (about 25 vol.%) for the smallest (0.05 g/g) binder ratio. As the binder ratio was increased, the volume fraction of un-granulated fines dropped down to effectively zero for the largest (0.25 g/g) binder ratio. Consequently, the original bi-modal particle size distribution became mono-modal, retaining only one inflex point corresponding to the granules (the inflex point corresponding to the primary particles disappeared with increasing binder ratio). This trend can be qualitatively explained as follows: assuming that each binder particle is able to collect a constant number of primary solid (mannitol) particles once molten, the number of binder particles present in the system for lower binder ratios (most notably, 0.05 and 0.11) is evidently not sufficient and leaves a significant proportion of the primary particles un-granulated. On the other hand, for the largest binder ratio (0.25), the number of binder seeds in the system is already large enough for essentially all of the primary particles to be collected and incorporated into granules. A quantitative explanation of the relationship between the fraction of un-granulated fines and the binder ratio, based on the material and number balance of binder particles, will be provided in the modelling section below (Eq. (9) in Section 3.3).

The second interesting trend revealed by Fig. 7 is that the size of the granules is affected by the binder ratio to a very small extent. The volume-weighted mean particle size corresponding to the four cases plotted in Fig. 7 was 692, 788, 789,

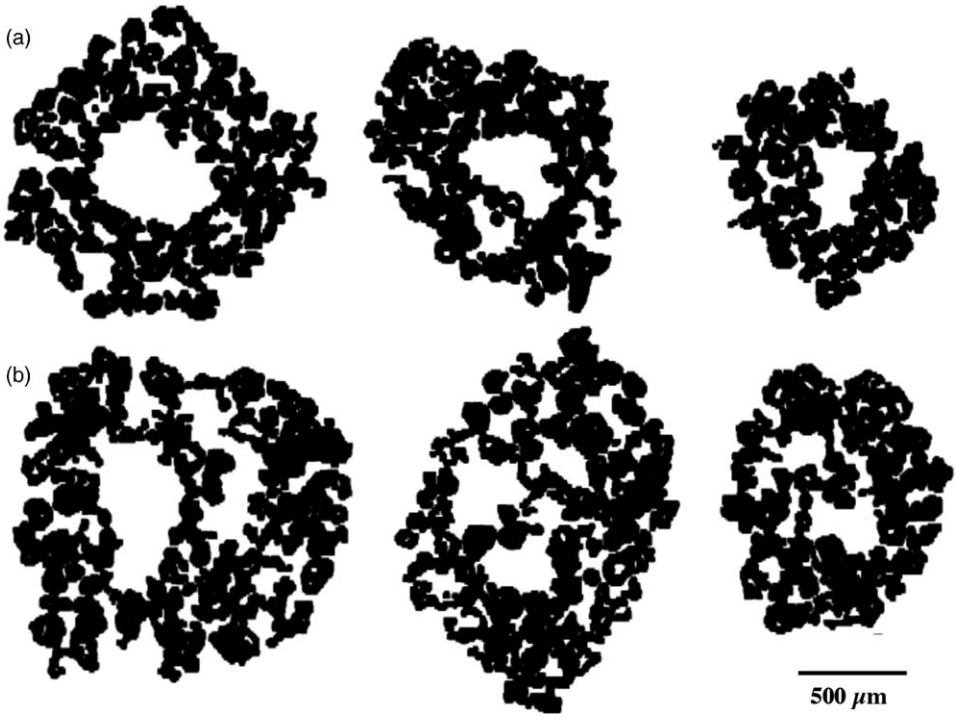


Fig. 6. Enhanced 2D horizontal X-ray images of mannitol granules prepared using L size (i.e., 355–500 μm) PEG binder. (a) Granules with a single core from three size classes; (b) selected multi-core granules.

and 802 μm, for binder ratio of 0.05, 0.11, 0.18, and 0.25 g/g, respectively. These values, however, have been evaluated from the entire PSD, i.e., including both granules and un-granulated fines. That is why the case with the largest fraction of fines gives the smallest mean particle size. Visually from Fig. 7 though, it is apparent that the PSD curves are practically identical once above the "fines" region. Indeed, when the mean particle size is calculated from PSD excluding the un-granulated primary particles (i.e., above 250 μm which is the upper limit of the primary particle size range), the values become 826, 812, 807, and 804 μm, respectively. These values then reflect the mean granule size, rather than that of a mixture of granules and un-granulated fines. Accounting for the experimental error, these four granule sizes can be regarded as practically identical (they are contained within ±1.4% of their average).

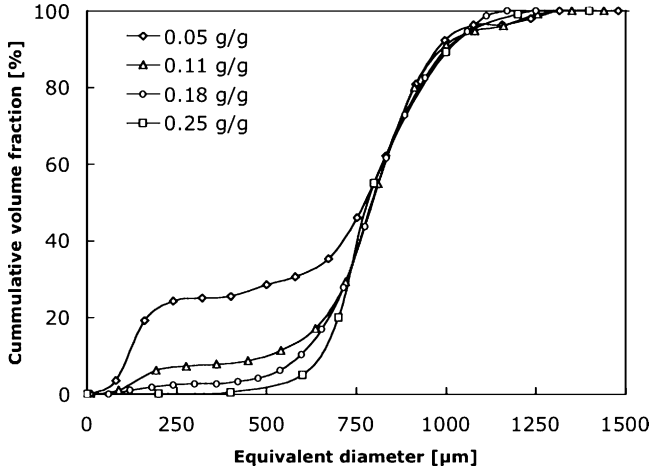


Fig. 7. Cumulative volume-weighted size distributions of granules prepared using L size binder and four different binder-to-solid ratios, as indicated in the legend.

In conclusion, it is possible to say from the combination of Figs. 3 and 7 that the size of the granules does not significantly depend on the binder-to-solids mass ratio, only on the binder particle size. This an important finding from the point of view of process control, and it is in stark contrast with "traditional" spray granulation where the final granule size generally very strongly depends on the binder-to-solids ratio; in fact, the binder ratio is often used as a manipulated variable to control the granule size (Cameron et al., 2005) in those cases. In our case, the granule size seems to have been fixed by the choice of the binder particle size, and the binder-to-solids mass ratio only controls the fraction of un-granulated fines.

### 3.3. Theoretical analysis

Let us now derive a relationship between the binder particle size and the resulting granule size in the ideal case of perfectly mono-disperse feed materials and granulation product. Let us assume that granules form by the immersion and layering growth mechanism depicted schematically in Fig. 8. According to this mechanism, the evidence for which was presented in Section 3.2 above, a single granule is formed from a binder particle by sequential deposition of primary solid particles on its molten surface. As the binder particle melts, the liquid is drawn by capillary forces to the shell region of the growing granule. The shell structure can be viewed as a random packing of the primary particles, partially saturated by the liquid binder. If the first layer of particles forms a stable arch and does not "implode" once the liquid

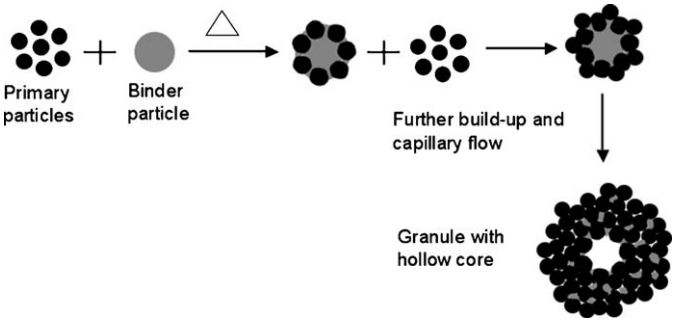


Fig. 8. Schematic illustration of a granule formation process by the immersion and layering mechanism.

from the core is depleted, a hollow-core granule is formed. The total amount of primary particles that can be accommodated in the shell depends on the total volume of binder initially available in the core.

Let us define

$$V_g = V_{core} + V_{shell} \quad (1)$$

to be the final granule volume. The core volume is related to the binder particle volume $V_b$ by

$$V_{core} = cV_b \quad (2)$$

where $0 \le c \le 1$ is the core volume compaction ratio. If the first layer of particles deposited on the surface of a partially molten binder particle formed a perfect, stable arch, then we would have $c = 1$. But in most actual situations one can expect the core to shrink somewhat as a result of impacts once the molten binder is redistributed by capillary action into the growing shell layer. The shell volume can be related to the binder particle volume by

$$V_{shell} = \frac{V_b}{\psi x_{b/s}} \quad (3)$$

where

$$\psi = \frac{V_{s,shell}}{V_{shell}} \quad (4)$$

is the volume fraction of primary solid particles in the shell, and

$$x_{b/s} = \frac{V_b}{V_{s,shell}} = x_{sat}\frac{1-\psi}{\psi} \quad (5)$$

is the volumetric binder/solids ratio in the shell, assuming all the binder from the core is eventually transported by capillary action into the shell. $x_{sat}$ is the relative pore-space saturation by the binder, and it can vary from the theoretical maximum of 1 (pores completely saturated by binder) to a minimum value $x_{sat}^{min}$, which corresponds to the minimum binder volume required for the formation of inter-particle bridges sufficiently strong to keep the granule together in the wet state. Substituting Eqs. (2), (3), and (5) into Eq. (1), we obtain

$$V_g = \left(c + \frac{1}{x_{sat}(1-\psi)}\right) V_b \quad (6)$$

which is the theoretical relationship between the granule volume and the binder particle volume. The equivalent granule diameter, $d_g$, can be calculated from the volume as $d_g = (6V/\pi)^{1/3}$. Assuming the parameters $c$, $\psi$, and $x_{sat}$ are constant, Eq. (6) suggests a linear relationship between the granule size and the binder particle size.

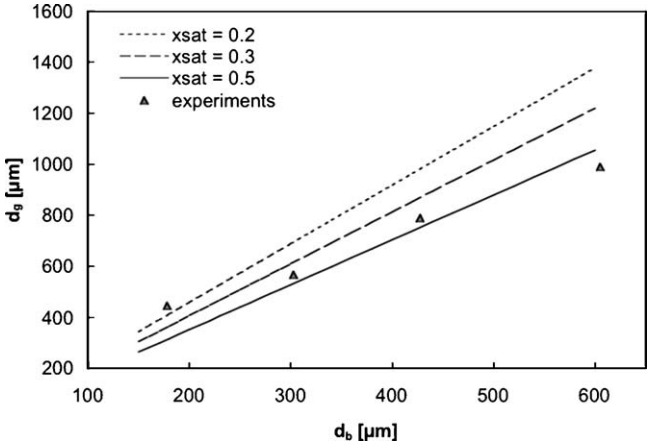


Fig. 9. Dependence of the mean granule diameter on the mean binder particle size predicted by the model (Eq. (6)) for $c = 1$ and $\psi = 0.55$, shown in the form of iso-saturation lines for three values of $x_{sat}$ as indicated in the legend, and compared with experimental data based on full distributions from Fig. 3.

This relationship is plotted in Fig. 9 for the limiting case of $c = 1$, $\psi = 0.55$ (loose particle packing), and three values of $x_{sat} = 0.2$, 0.3, and 0.5. For comparison the graph also contains experimental data points of the mean granule size obtained from the four different binder particle sizes S, M, L, and XL (the full granule size distributions are shown in Fig. 3). As can be seen in Fig. 9, although there is clearly a direct correlation between the binder particle size and the granule size, the experimental points do not fall on a single iso-saturation line. This means that one or more of the three parameters $c$, $\psi$, and $x_{sat}$ must also vary as function of the binder particle size $d_b$. We have used Eq. (6) to carry out a parametric sensitivity study which showed that the core compaction ratio $c$ has a very small effect on the slope of the lines in Fig. 9, whereas both $\psi$ and $x_{sat}$ have a strong influence. Since $\psi$ is the particle packing density in the shell region, there is little physical reason for it to be dependent on the binder particle size—it may be different than the 0.55 value initially chosen for Fig. 9, but it should be independent of $d_b$. This leaves the relative pore-space saturation as the only adjustable parameter. Indeed it is not unreasonable to assume that for larger binder particles the relative pore saturation of the shell region is somewhat higher, as is required to explain the data in Fig. 9, since more binder is available from the core.

The second relationship of interest is between the total binder/solids mass ratio and the fraction of un-granulated fines. In the derivation we will again assume an idealised situation, i.e., that the primary solid particles are either part of a granule of volume $V_g$ given by Eq. (6), or they are completely un-granulated. Let us define the volume fraction of un-granulated fines in the product as

$$w_{fines} = \frac{V_{fines}}{V_{fines} + V_g} \quad (7)$$

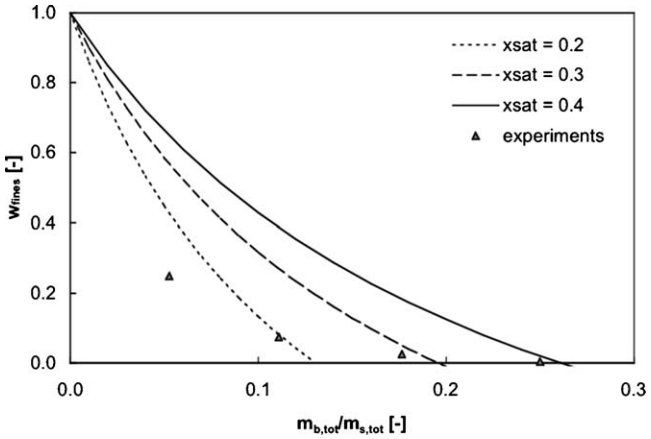


Fig. 10. Dependence of the mass fraction of un-granulated fines on the total binder to solids mass ratio predicted by the model (Eq. (9)) for $c = 1$ and $\psi = 0.55$, shown in the form of iso-saturation lines for three values of $x_{sat}$ indicated in the legend, and compared with experimental data based on full distributions from Fig. 7.

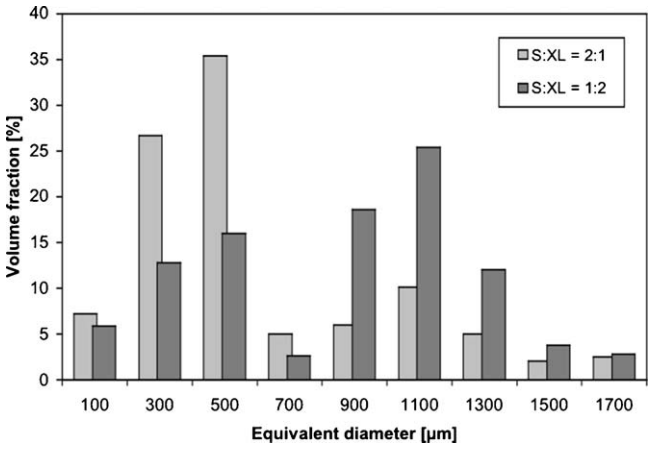


Fig. 11. Bi-modal size distribution of granules produced by using a mixture of PEG binder particles from two size ranges, S (106–250 μm) and XL (500–710 μm), mixed in a 2:1 and a 1:2 ratio by mass as indicated in the legend. The overall binder/solids ratio was 0.18 in both cases.

where $V_{fines}$ is the volume of un-granulated primary solid particles and $V_g$ is the granule volume given by Eq. (6). $V_{fines}$ can be related to the total volume of primary solid particles and the binder volume using Eqs. (4) and (5), i.e.,

$$V_{fines} = V_{s,tot} - V_{s,shell} = V_{s,tot} - \frac{\psi}{(1-\psi)x_{sat}} V_b \quad (8)$$

After substitution of Eq. (8) in to Eq. (7) and rearrangement, we obtain a relationship between the total binder/solids mass ratio and the volume fraction of un-granulated fines in the following form

$$w_{fines} = \frac{1 - (\psi/(1-\psi)x_{sat})(m_{b,tot}/m_{s,tot})(\rho_s/\rho_b)}{1 + (c + (1/x_{sat}))(m_{b,tot}/m_{s,tot})(\rho_s/\rho_b)} \quad (9)$$

where $\rho_s$ and $\rho_b$ are the density of the primary solids and the binder, respectively. Notice that Eq. (9) is a rational function of the binder/solids mass ratio, and that it contains the same three a priori unknown parameters as Eq. (6), namely $c$, $\psi$, and $x_{sat}$. In Fig. 10, we plot $w_{fines}$ calculated from Eq. (9) as function of the total binder/solids mass ratio for the case $c = 1$ and $\psi = 0.55$ (same as in Fig. 9) and three values of pore space saturation, $x_{sat} = 0.2$, 0.3, and 0.4. Experimental data for L size binder and four different total binder/solids ratios are also shown in Fig. 10 for comparison (the full volume-weighted distributions from which the data points are calculated are shown in Fig. 7). Here fines were defined as particles smaller than 350 μm as no mannitol primary particles could be larger than this value (cf. Table 1). Similarly as in Fig. 9, we can see that although the theoretical curves calculated using Eq. (9) predict qualitatively correct trends, no single iso-saturation line passes through all the data points. This means that, as was the case with Eq. (6), we must allow for $x_{sat}$ to be variable and dependent on the binder to solids mass ratio, $m_{b,tot}/m_{s,tot}$. Parametric sensitivity with respect to $c$ was again very low, while $\psi$ was found to have an effect on the shape of the curves and could therefore be used as an additional adjustable parameter – but again there is no physical reason for $\psi$ to be variable as function of $m_{b,tot}/m_{s,tot}$. As can be seen in Fig. 10, in order to explain the experimental data the pore-space saturation $x_{sat}$ must increase with increasing binder/solids ratio. This may well be the case; as more binder is available, a higher proportion of the inter-particle pore-space within the granule shell can be filled by the binder.

### 3.4. Granules with custom size distribution

Finally, let us demonstrate how the direct dependence of mean granule size on the binder particle size, discussed above, can be used for the production of granules with a priori specified size distribution. Granules were prepared according to the protocol described in Section 2.1, with a constant binder/solids mass ratio of 0.18 but using a binary mixture of S and XL size binder particles instead of only one size. The proportion of S-size binder particles in the mixture was systematically varied from 0 to 1. Whenever both binder sizes were present, the resulting granules had a characteristic bi-modal size distribution, an example of which is shown in Fig. 11 for two S:XL ratios. The minimum between the two modes was around 800 μm in all cases, and the maxima corresponding to S- and XL-seeded granules were on average at 410 and 1050 μm, respectively. Notice that these values are very close to data presented in Fig. 3, where the volume-mean granule diameters of 445 and 989 μm were obtained for granules prepared from pure S and XL binder particles, respectively, and the same total binder/solids ratio.

This result suggests that the growth processes on the S and XL seeds occur in parallel and are essentially independent from each other, which means that the resulting bi-modal size distribution should be simply a linear combination of the mono-modal distributions for S and XL seeds. In order to confirm this hypothesis, the cumulative volume fraction of granules smaller than 800 μm (the minimum separating the two modes) was evaluated from all experiments with variable S:XL ratio and plotted against the mass fraction of S-size particles in the binder mix. This plot is shown in Fig. 12; for comparison, the line denoting direct proportionality is drawn in the graph along with the experimental data points. One can see that indeed the fraction

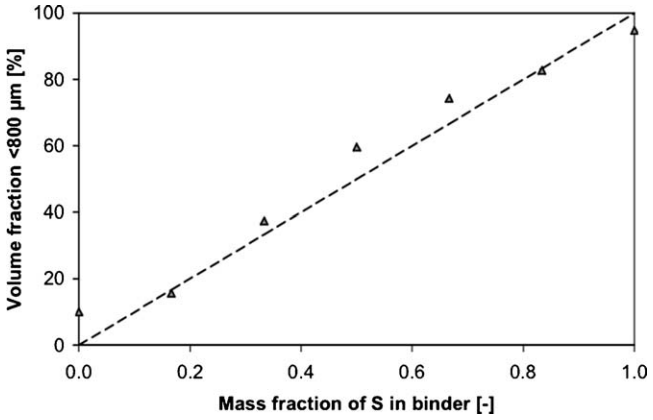


Fig. 12. Volume fraction of granules smaller than 800 μm evaluated from bi-modal size distributions realised by changing the proportion of S-size binder particle in the binder mix (S and XL). The overall binder/solids ratio was 0.18 in all cases. Triangles are experimental data points, the dashed line has a slope of 100.

of granules belonging to the smaller mode is directly proportional to the mass fraction of the smaller particles in the binder mix. From this we can conclude that by using the in situ melt fluid bed granulation method described in this work (and possibly other granulation methods where large binder particles or droplets are used as seeds), it is possible to prepare granules with "designed" size distribution, just by mixing binder particles of the appropriate size in the required ratio.

## 4. Conclusions

The role of binder particle size and binder/solids ratio on granule formation in fluid-bed in situ melt granulation has been studied. The final granule size was found to be an increasing function of the binder particle size; however for a given binder mass the increase in binder size may result into larger number fraction of un-granulated fines. Binder size was also found to have strong influence on the particle build-up mechanism; the formulations that contain binder particles sufficiently larger than the size of primary solids tend to produce granule structures with a hollow core. For a given granule size class, the core size appears to increase with the binder particle size, which offers the possibility of controlling granule structure and hence the application properties such as dissolution and tabletting. X-ray micro-tomography has proved to be a useful technique to characterise not only the granule structures but also to elucidate the likely granulation mechanism. The established dependence of granule size on binder particle size was used for the preparation of granule batches with a priori designed, bi-modal size distribution.

Theoretical analysis of the in situ melt granulation process, based on the immersion and layering growth mechanism depicted in Fig. 8, yielded relationships (Eqs. (6) and (9)) that allow the estimation of the mean granule size and the fraction of un-granulated fines as function of the binder particle size and the binder to solids mass ratio, provided that two parameters are known: the primary particle packing density in the granule shell, $\psi$, and the relative pore-space saturation by the binder, $x_{sat}$. These quantities can either be regarded as adjustable and obtained by least-square regression from experimental data, or they could in principle also be evaluated directly by microstructure analysis of the granule X-ray images. The latter approach was not possible in our specific case due to very close X-ray attenuation coefficients of mannitol and PEG-6000, but for other systems, as was shown in our recent work (Ansari and Stepanek, in press), the image segmentation into primary solid particles and binder phase can be done.

## Acknowledgments

We would like to thank Dr. Judith Bonsall and Mr. Steve Kynaston from Unilever R&D Port Sunlight for kindly providing the X-ray imaging facility. Funding for this research has been provided by the UK Engineering and Physical Sciences Research Council through grant no. GR/S69146/01.

## References

Abberger, T., 2001. Influence of binder properties, method of addition, powder type and operating conditions on fluid-bed melt agglomeration and resulting tablet properties. Pharmazie 56, 949–952.

Abberger, T., Seo, A., Schæfer, T., 2002. The effect of droplet size and powder particle size on the mechanisms of nucleation and growth in fluid bed melt agglomeration. Int. J. Pharm. 249, 185–197.

Ansari, M.A., Stepanek, F. The effect of granule microstructure on dissolution rate. Powder Technol., in press.

Bogner, R.H., Wilkosz, M., 2002. Fast-dissolving tablets: new dosage convenience for patients. U. S. Pharm. 27, 34–43.

Cameron, I.T., Wang, F.Y., Immanuel, C.D., Stepanek, F., 2005. Process systems modelling and applications in granulation: a review. Chem. Eng. Sci. 60, 3723–3750.

Farber, L., Tardos, G., Michaels, J.N., 2003. Use of X-ray tomography to study the porosity and morphology of granules. Powder Technol. 132, 57–63.

Iveson, S.M., Litster, J.D., Hapgood, K., Ennis, B.J., 2001. Nucleation, growth and breakage phenomena in agitated wet granulation processes: a review. Powder Technol. 117, 3–39.

Kaushik, D., Dureja, H., Saini, T.R., 2004. Mouth dissolving tablets: a review. Ind. Drugs 41, 187–193.

Litster, J.D., 2003. Scale-up of wet granulation processes: science not art. Powder Technol. 130, 35–40.

Mort, P., 2005. Scale-up of binder agglomeration processes. Powder Technol. 150, 86–103.

Schæfer, T., Mathiesen, C., 1996. Melt pelletization in a high shear mixer: IX. Effects of binder particle size. Int. J. Pharm. 139, 139–148.

Schæfer, T., Wørts, O., 1978. Control of fluidized bed granulation: IV. Effects of binder solution and atomization on granule size and size distribution. Arch. Pharm. Chem. Sci. Ed. 6, 14–25.

Turton, R., Tardos, G.I., Ennis, B.J., 1999. Fluidized bed coating and granulation. In: Yang, W.C. (Ed.), Selected Topics on Fluidization, Solids Handling and Processing. Noyes Publications, Park Ridge, pp. 331–429.

Walker, G.M., Holland, C.R., Ahmad, M.M.N., Craig, D.Q.M., 2005. Influence of process parameters on fluidised hot-melt granulation and tablet pressing of pharmaceutical powders. Chem. Eng. Sci. 60, 3867–3877.